ELSEVIER

Journal of Power Sources 102 (2001) 277–282

JOURNAL OF POWER SOURCES

www.elsevier.com/locate/jpowsour

DEMS study of gas evolution at thick graphite electrodes for lithium-ion batteries: the effect of γ-butyrolactone

Martin Lanz[1], Petr Novák*

Laboratory for Electrochemistry, Paul Scherrer Institute, CH-5232 Villigen PSI, Switzerland

Received 30 March 2001; accepted 7 May 2001

Abstract

Differential electrochemical mass spectrometry (DEMS) was used to study the reductive decomposition of an electrolyte based on ethylene carbonate/dimethyl carbonate (EC/DMC), as well as the formation of a solid electrolyte interphase (SEI) in this electrolyte, at thick (75–100 μm) porous graphite composite electrodes. A number of graphite electrodes differing in their electrochemical lithium intercalation properties were investigated in potential-sweep experiments. They proved to be similar with respect to the evolution of ethylene and hydrogen gas during the first two charge/discharge cycles. Due to an incomplete coulombic conversion, a high irreversible capacity, as well as slow diffusion kinetics and an enhanced ohmic resistance of the electrodes, SEI formation on these thick electrodes was not yet *complete* after the first charge/discharge cycle. Undesired gas evolution can be reduced by adding γ-butyrolactone (GBL) as an electrolyte co-solvent. The amount of ethylene and hydrogen gas evolved decreases with increasing percentages of GBL in an EC/DMC electrolyte, indicating that the SEI layer is built up from GBL rather than from EC decomposition products.

Keywords: In-situ DEMS study; Lithium-ion batteries; Graphite electrodes; Electrolyte decomposition; Carbonate electrolytes; γ-Butyrolactone

1. Introduction

Lithium-ion rechargeable batteries currently available in the consumer market often contain a graphite composite negative electrode. Irreversible capacity losses occurring mainly in the first charging cycle (lithium insertion into the graphite) are still a challenge, since they substantially reduce the energy density of the cell. This reduction in cell capacity is due to a reductive degradation of the carbonate electrolyte and to the consumption of Li^+ ions for the formation of a protective solid electrolyte interphase (SEI) on the negative electrode [1,2]. The degradation process is attended by the formation of volatile by-products. An objective of current research is the development of electrolytes that favour the formation of a stable SEI while minimising the decomposition reactions and lithium consumption accompanying this process. This would not only lead to a lower irreversible capacity of the graphite electrodes in the first charging cycle but would also diminish gas evolution during the formation cycle, which is a potential problem in the fabrication of lithium-ion batteries.

We recently used differential electrochemical mass spectrometry (DEMS) when studying the processes of electrolyte decomposition and SEI formation, and observed the formation of ethylene and propylene as well as hydrogen gas on thin graphite electrodes (<10 μm; ~0.5 mg/cm^2) in different carbonate-based electrolyte solutions [3,4]. DEMS is a powerful tool for identifying in-situ the gaseous and volatile products formed in an electrochemical reaction [5]. A non-wettable, porous membrane is inserted as a solvent barrier between an electrochemical cell and the vacuum system of a mass spectrometer. A porous working electrode is deposited onto the membrane. Volatile reaction products are pumped off continuously during the electrochemical reaction, and can be analyed with the mass spectrometer.

The present work focussed on gas evolution at thick graphite electrodes for lithium-ion batteries under initial charging. The general gas evolution behaviour of various graphites and thick, porous electrodes (75–100 μm; ~5–7 mg/cm^2) was investigated in an ethylene carbonate/dimethyl carbonate (EC/DMC) electrolyte [6,7]. The effect of γ-butyrolactone (GBL) as a co-solvent diminishing the gas evolution in EC/DMC electrolyte solutions was semi-quantitatively elucidated.

* Corresponding author. Tel.: +41-56-310-24-57; fax: +41-56-310-44-15.
E-mail address: petr.novak@psi.ch (P. Novák).
[1] Present address: Mettler-Toledo GmbH, CH-8603 Schwerzenbach, Switzerland.

0378-7753/01/$ – see front matter
PII: S0378-7753(01)00826-6

2. Experimental

In the experiments without γ-butyrolactone, 1 M $LiPF_6$ dissolved in EC/DMC (1:1 w/w; battery electrolyte Merck LP 30, Selectipur) was used as an electrolyte. The H_2O content was determined by Karl–Fischer titration, and found to be <10 ppm, while the HF content was about 50 ppm. In the experiments involving GBL as a co-solvent, $LiBF_4$ (Stella, 1 M solutions) was used as the salt, because the $LiPF_6$/GBL combination was reported to have an adverse effect on the cyclability of graphite [8]. All solvent mixtures contained a constant fraction (50 wt.%) of EC, a variable percentage of GBL (0, 5, 25 or 50 wt.%), and a complementary percentage of DMC (all solvents from Merck, Selectipur grade). The H_2O content of the electrolytes was ca. 20 ppm. The electrolytes were stored and handled in an argon-filled glove box.

The DEMS setup has been described in [3,4,6]. In short, it consisted of an electrochemical cell where the working electrode active material was deposited on a Gore-Tex ePTFE membrane (pore size 0.02 μm). This membrane was the interface between the cell and the vacuum system of a quadrupole mass spectrometer. The active surface area of the working electrode was 0.5 cm^2. Electrical contact with the working electrode was established through aluminium foil directly attached to the graphite layer at the periphery of the graphite-coated membrane, outside the electrolyte-wetted area. Metallic lithium was used as the counter and reference electrode. All potentials are given with reference to the Li/Li^+ couple in the electrolyte used.

The procedure for preparing the working electrode has been described before [3,4]. Different graphite powders were investigated: TIMREX SFG 6, TIMREX SFG 15, TIMREX SLM 44 (all from TIMCAL Group, Switzerland), and a purely hexagonal graphite sample, prepared as described in [9]. The amount of graphite/binder composite electrode material deposited on the membrane was a few mg/cm^2. This loading corresponds to that typically used in commercial lithium-ion cells of 6–15 mg/cm^2 [10]. The thickness of the graphite electrodes was measured with a micrometer screw. The porosity of the electrodes was calculated from the loading and the thickness, and found to be about 70%. Electrodes with a lower porosity are used for industrial lithium-ion batteries, where 40–50% porosity [11] should be considered as an upper limit.

All measurements were carried out at room temperature. At the beginning of a potential-controlled DEMS experiment, the potential was decreased with a scan rate of 4 mV/s from an open-circuit value (of about 3.2 V) to 2.0 V versus Li/Li^+. At 2.0 V, the current was allowed to decrease to a value of <30 μA, then the graphite electrode was cycled between 2.0 and 0.01 V versus Li/Li^+ with a scan rate of 0.4 mV/s. The current (cyclic voltammogramme, CV) and the mass signals (mass spectrometric cyclic voltammogramme, MSCV) were recorded simultaneously as functions of the electrode potential.

3. Results and discussion

3.1. DEMS behaviour of thick graphite electrodes

Fig. 1 shows the results of cyclic potential-sweep DEMS experiments performed with three different graphites using

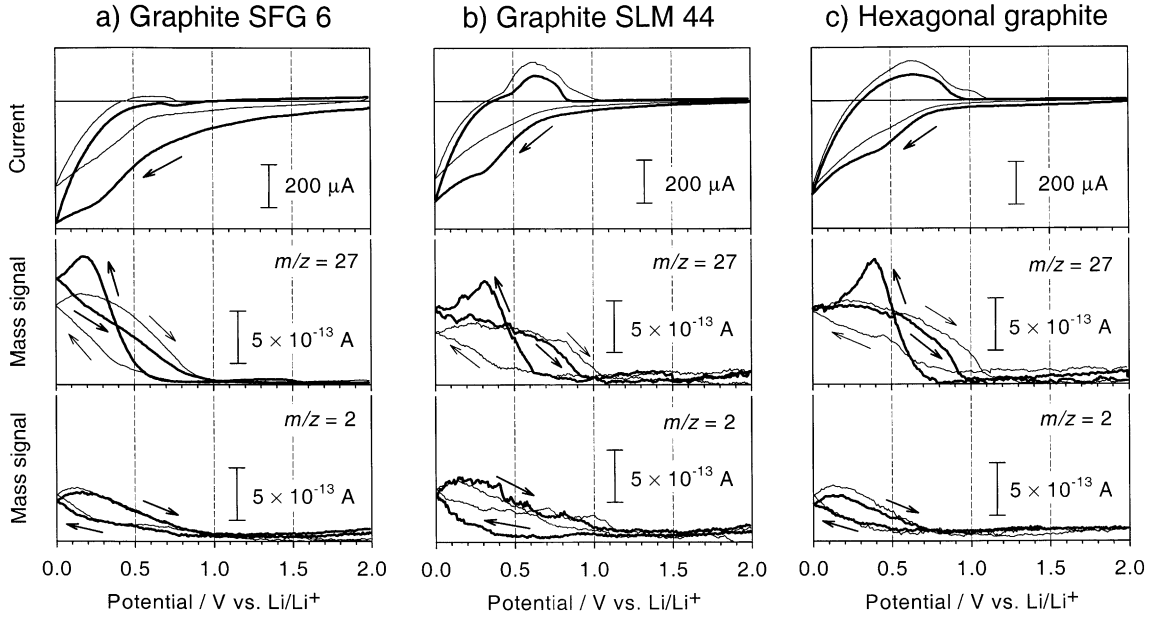

Fig. 1. CVs and MSCVs recorded for graphites SFG 6 (a), SLM 44 (b), and a hexagonal graphite sample (c), in 1 M $LiPF_6$/EC/DMC. The electrode loading was 2.3 mg (a) or 3.3 mg (b and c) of graphite/binder composite on an electrode area of 0.5 cm^2. The MSCVs with $m/z = 27$ represent ethylene, those with $m/z = 2$ represent hydrogen. The scan rate was 0.4 mV/s; the first (bold trace) and second (fine trace) cycles are shown.

Table 1
Graphites used for DEMS experiments[a]

Graphite	Specific surface area (m^2/g)[b]	Particle size d_{50} (μm)[c]	Irreversible specific charge (%)[d]
TIMREX SFG 6	15.2	3.4	21
TIMREX SLM 44	4.5	24.0	8
Hexagonal graphite[e]	2.8	27.5	∼60
TIMREX SFG 15	8.5	7.5	14

[a] Values were taken from [9,12].
[b] Brunauer–Emmett–Teller (BET) specific surface area.
[c] Median of the particle size distribution; 50% of the graphite particles are smaller than the d_{50} value.
[d] The percentage values of the irreversible specific charge (irreversible capacity) are given with respect to the total specific charge (total capacity) in the first cycle.
[e] Hexagonal graphite crystal structure: the sequence of graphene layers is ABABAB; rhombohedral structure: the sequence is ABCABC.

electrode loadings of 4.5 mg/cm^2 (Fig. 1a; thickness ∼75 μm) or 6.6 mg/cm^2 (Fig. 1b and c; thickness ∼100 μm) of the graphite/binder composite. The first and second scan cycles are shown in each case. The MSCVs with $m/z = 27$ represent ethylene, those with $m/z = 2$ represent hydrogen evolution. Three graphites with different electrochemical properties were chosen for the investigation: TIMREX SFG 6, TIMREX SLM 44, and a purely hexagonal graphite sample with no rhombohedral parts in its crystal structure. Table 1 gives an overview of the graphites investigated. Graphite SLM 44 is well suited for practical lithium-ion cells, while graphite SFG 6 and the hexagonal graphite have irreversible capacities too large for practical purposes. In the case of graphite SFG 6, the large irreversible capacity is due to its large specific surface area [12–14], but in the case of hexagonal graphite, the large irreversible capacity is due to a partial exfoliation of the graphene layers during lithium intercalation [9,15–17].

The general gas evolution behaviour observed in Fig. 1a–c was as follows. In the first charging half-cycle (lithium insertion into the graphite electrode), ethylene evolution started at a potential of about 0.7–0.8 V versus Li/Li$^+$ and went through a maximum at about 0.2–0.4 V. The gas evolution then decreased, but continued during the following discharging half-cycle (lithium extraction from the graphite electrode) as long as the potential was more negative than about 1.0 V. The fact that in the reverse sweep, gas evolution appears to continue beyond its onset potential observed in the forward sweep, can be accounted for by a slow diffusion of ethylene gas through the thick graphite electrode. This was confirmed in a potential step experiment (not shown here), where we found that the ethylene signal decreased to zero within about 10 min after the potential of the graphite electrode had been stepped from 0.4 V (gas evolution) to 1.4 V (no gas evolution). Further ethylene evolution occurred during the second charge/discharge cycle (see Fig. 1a–c), however, it did not give rise to a distinct peak such as that observed in the first cycle. Hydrogen evolution was observed to similar extents in the first and second cycle, always starting and ending at a potential more negative than about 1 V versus Li/Li$^+$. No volatile decomposition products other than ethylene and hydrogen were observed. As seen from Fig. 1, the gas evolution behaviour was similar for the three graphites investigated. Thus, the large specific surface area of graphite SFG 6 or the partial exfoliation of the hexagonal graphite did not visibly affect ethylene or hydrogen evolution during the DEMS experiment.

In the CVs of Fig. 1a–c, re-oxidation currents in the first discharging half-cycles are small. This implies that the coulombic efficiency of lithium insertion/extraction was small in the first charge/discharge cycle in these relatively fast experiments. A scan rate of 0.4 mV/s was in fact selected as the best compromise from the point of view of the signal-to-noise ratio of the mass signals. Most of the current consumed during the reductive part of the voltammetric sweep contributed to electrochemical reduction of the carbonate electrolyte and to the direct or indirect formation of a SEI layer on the graphite electrode. Electrochemical lithium insertion into the graphite electrode was not yet complete at the end of the reductive part of the voltammetric sweep. For example, in the case of graphite SFG 6 (Fig. 1a), only 44% of the theoretical amount of charge for a reversible, full loading of the graphite with lithium up to the formal composition of LiC_6 (372 Ah/kg of graphite, [18]) was injected during the first voltammetric sweep, and all of this current was used up for SEI formation. In contrast to graphite SFG 6, graphite SLM 44 and the hexagonal graphite gave pronounced re-oxidation current peaks during the first discharging half-cycle (see Fig. 1a–c). Thus, for samples with a lower specific surface area, the irreversible capacity decreased, and lithium insertion became more important relative to SEI formation.

Gas evolution on thick graphite electrodes differs from that on thinner ones. In our earlier DEMS studies [3,4] on thin SFG 6 graphite electrodes (<10 μm; ∼0.5 mg/cm^2), ethylene was only evolved within a narrow potential window between about 0.8 and 0.3 V versus Li/Li$^+$ in the first reduction half-cycle, which nicely correlated with a cathodic current peak in the CV corresponding to SEI film formation on the graphite electrode. In the re-oxidation scan and subsequent scans no ethylene was detected. The total charge injected during the reductive part of the first cycle was approximately 80% of reversible coulombic conversion (i.e. reversible lithium insertion up to LiC_6) of the graphite electrode; about one fifth of this charge was re-extracted in the oxidative half-cycle. Thus, thin graphite electrodes exhibited much higher irreversible capacities in the DEMS cell than in conventional lithium-ion cells [12–14]. In the present experiments on thick electrodes (∼75–100 μm; 4.5–6.6 mg/cm^2), however, the coulombic conversion was even lower, and the irreversible capacity was higher, and both ethylene gas evolution and SEI formation extended beyond the first charging half-cycle. A number of reasons can be cited for this behaviour.

1. At thick graphite electrodes, electrochemical reaction kinetics is governed by a long duration of the diffusion of the reactants within the electrodes. The lithium and EC consumed in the pores of the graphite electrode during SEI film formation and Li intercalation are not replenished quickly enough from the bulk electrolyte solution to sustain fast electrochemical reactions. At thin graphite electrodes, on the other hand, the SEI is rapidly formed while the kinetics of lithium insertion into the graphite might be a rate-determining factor at the relatively fast charging rate of the DEMS experiment.
2. The irreversible capacity of graphite in a DEMS cell is higher than that in a conventional lithium-ion cell, because (i) the electrolyte to graphite ratio in the DEMS cell is extremely high, which brings about a larger amount of electrolyte impurities, e.g. trace water, that are reduced on the graphite electrode and increase the measured irreversible charge consumption. Further, (ii) SEI formation is perturbed by gas depletion. Moreover, (iii) the porosity of the graphite electrode was higher than that found in a lithium-ion cell (see Section 2), which might also affect the SEI buildup.
3. The ohmic resistance in the DEMS cell is substantial. From current interruption measurements on the graphite electrodes (see Fig. 8 of [7]) and from earlier DEMS investigations [19], the estimated overall ohmic resistance of the DEMS cell was of the order of a thousand ohms. Part of the corresponding voltage drop (up to several hundred millivolts) might occur across the electrode. As a test for the influence of lateral conductivity of the graphite electrodes, a fine nickel grid was pressed into the ePTFE membrane before depositing the graphite composite. This DEMS experiment gave the same results as those obtained without grid, showing that the lateral conductivity was sufficient in the electrodes without grid. Major part of the ohmic resistance in a graphite electrode depends on the insulating and passivating properties of the SEI film formed on the graphite [20], which in turn is related to the irreversible capacity and the porosity of the electrode.

In summary, the differences in behaviour of thick and thin graphite electrodes in a DEMS cell are due to nonidealities of the thick electrodes. This does not detract from their utility in certain studies. Thus, experiments on thick graphite electrodes producing significantly more gas than thin ones are quite useful for the investigation of strategies by which to minimise the amount of gas evolved. The power of this approach is documented below with an electrolyte system containing GBL as a co-solvent.

3.2. γ-Butyrolactone as a carbonate electrolyte co-solvent

In the search for organic solvents suited for lithium-ion batteries with graphite or carbon anodes, GBL has received renewed attention recently. It was investigated as a solvent or as a co-solvent with EC. With $LiBF_4$ as the electrolyte salt, it exhibited good cycling stability, both in liquid electrolyte lithium-ion batteries [21,22] and in gel–polymer electrolyte lithium-ion batteries [23–25]. However, the utility of GBL as an electrolyte co-solvent for lithium-ion batteries appears to be limited to specific electrolyte compositions. We recently observed that the cyclability of a graphite electrode in mixed EC/DMC/GBL electrolytes strongly depended on the electrolyte salt [8]. With $LiBF_4$ as the electrolyte salt, the cyclability was significantly better than with $LiPF_6$ or $LiClO_4$ [8].

As a solvent, GBL has the advantages of a low freezing point (−44°C) and high boiling point (204–206°C), and electrolytes containing GBL exhibit high ionic conductivities [21,22,24,26]. We chose to investigate GBL as a co-solvent for EC or EC/DMC electrolytes in terms of gas evolution at graphite electrodes for lithium-ion batteries under initial charging. TIMREX SFG 15 was the graphite chosen for these experiments, since in its properties (specific surface area, particle size, irreversible specific charge), it is an intermediary among the graphites investigated above (see Table 1).

Figs. 2 and 3 show the results of a series of DEMS experiments on graphite SFG 15 (electrode loading ca. 2.9 mg/cm^2) in 1 M $LiBF_4$ electrolytes prepared with

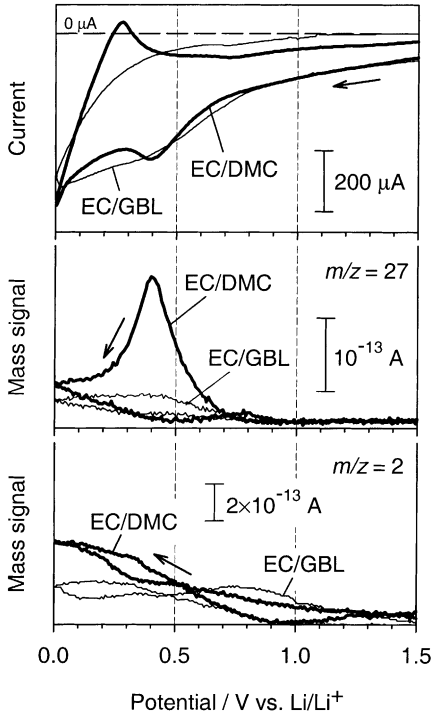

Fig. 2. CV and MSCVs recorded for graphite SFG 15 in 1 M $LiBF_4$ electrolytes prepared from EC/DMC (1:1, bold trace) and EC/GBL (1:1, fine trace), respectively. The electrode loading was ca. 1.5 mg of graphite/binder composite on an electrode area of 0.5 cm^2. The MSCVs with $m/z = 27$ represent ethylene, those with $m/z = 2$ represent hydrogen. The scan rate was 0.4 mV/s. The first scan cycle of a fresh electrode is shown for each electrolyte composition.

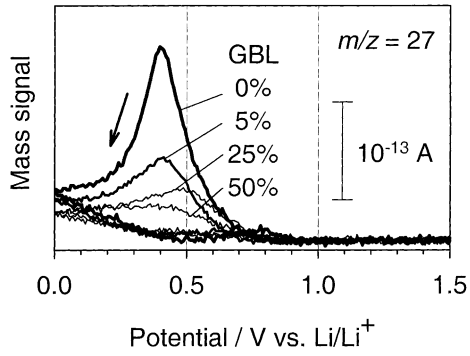

Fig. 3. MSCVs with $m/z = 27$ representing ethylene, recorded for graphite SFG 15 in 1 M $LiBF_4$ electrolytes prepared from EC/DMC/GBL mixed solvents. The composition of the solvent was varied from 0 to 50 wt.% GBL, with a constant fraction of EC (50 wt.%). The experimental parameters were the same as in Fig. 2.

EC/DMC/GBL mixed solvents. The solvent composition was varied from 0 to 50 wt.% GBL, always with a constant fraction of 50 wt.% EC. Fig. 2 represents the 'end members' of this measurement series, i.e. the experiments with 0 wt.% GBL (pure EC/DMC electrolyte) and 50 wt.% GBL (pure EC/GBL electrolyte), respectively. The CVs as well as the MSCVs for ethylene ($m/z = 27$) and hydrogen ($m/z = 2$) evolution at fresh graphite electrodes are displayed. Fig. 3 illustrates the ethylene ($m/z = 27$) evolution behaviour of fresh graphite electrodes for the whole measurement series, i.e. in EC/DMC/GBL electrolytes with 0, 5, 25 or 50 wt.% GBL.

The general features observed in the experiment with the EC/DMC electrolyte in Fig. 2 correspond to those of thick graphite electrodes as shown in Fig. 1. The CV for the EC/DMC electrolyte in Fig. 2 reveals a distinct, broad cathodic current peak around 0.4 V which nicely correlates with the ethylene gas evolution peak in the MSCV. These features are more pronounced in the EC/DMC experiment of Fig. 2 than in Fig. 1, the reason being a lower electrode coverage in case of Fig. 2. Both the cathodic current peak and the ethylene gas evolution are due to SEI formation occurring at this stage of the potential sweep. Eqs. (1) and (2) provide a simple description of SEI formation and ethylene gas evolution occurring under EC decomposition at graphite electrodes [4]

$$2EC + 2Li^+ + 2e^- \rightarrow (CH_2OCO_2Li)_2 \downarrow_{(SEI)} + CH_2{=}CH_2 \uparrow \quad (1)$$

$$EC + 2Li^+ + 2e^- \rightarrow Li_2CO_3 \downarrow_{(SEI)} + CH_2{=}CH_2 \uparrow \quad (2)$$

A large difference is seen between the experiment with EC/GBL and EC/DMC electrolyte in Fig. 2. In the EC/GBL electrolyte, almost no ethylene gas was evolved, while the cathodic current peak in the CV reduced to a mere, broad shoulder in the curve. The EC content of the electrolyte solution was the same in these two experiments (50 wt.%). Therefore, we find that replacing DMC by GBL as a co-solvent for EC has the effect of considerably reducing ethylene gas evolution from EC. The full series of experiments illustrated in Fig. 3 shows how the amount of evolved ethylene gas changes with the percentage of GBL present in the EC/DMC/GBL electrolyte. The MSCVs for $m/z = 27$ in Fig. 3 show that ethylene gas evolution was strongest in the pure EC/DMC electrolyte (0 wt.% GBL), and it decreased with increasing GBL percentage, i.e. in the order $0 > 5 > 25 > 50$ wt.% GBL. Hydrogen evolution ($m/z = 2$) also decreased with increasing GBL percentage in the electrolyte solution (see Fig. 2). However, here the trend was less pronounced than in ethylene evolution (see Fig. 2). Gases other than ethylene and hydrogen were not detected.

The results of Figs. 2 and 3 demonstrate that GBL, when used as a co-solvent in an EC or EC/DMC electrolyte, strongly represses ethylene gas evolution as a reaction accompanying SEI formation. We deduce that in the presence of GBL, the SEI film is built up in a different way. More specifically, less EC is decomposed in the presence of GBL. Apparently, decomposition products of GBL replace those of EC in the SEI layer. Since a distinct cathodic current peak, such as that observed with the EC/DMC electrolyte, was not observed in the case of EC/GBL (see Fig. 2), we presume that GBL decomposition takes place over a broader electrode potential range than EC decomposition. These assumptions are supported by the following observations. (i) Koike et al. [27] have shown with an electrochemical quartz crystal microbalance that electrolytes made of GBL/$LiPF_6$ form dense, protective SEI surface layers. (ii) Aurbach and coworkers have demonstrated that reductive GBL decomposition mainly produces the cyclic γ-alkoxy-β-keto ester Li salt as shown in Fig. 4 [28–32], or in the presence of water, γ-hydroxy Li butyrate [$HO(CH_2)_3$-COOLi] [28–32]. (iii) We recently performed electrochemical cycling tests on graphite SFG 15 electrodes in electrolytes prepared from mixtures of EC with DMC and GBL and different salts, namely, $LiBF_4$, $LiPF_6$ or $LiClO_4$ [8]. The cyclability of the graphite and the irreversible specific charge of the graphite in the first charge/discharge cycle (formation cycle) depended on solvent composition. Additionally, when GBL was used as an electrolyte co-solvent, the electrochemical properties of the graphite strongly depended on the electrolyte salt. Good cyclability was only obtained when $LiBF_4$ was used as the electrolyte salt. When $LiPF_6$ or $LiClO_4$ were used instead, a fast capacity fading of the graphite anode was observed in the cycling tests [8]. These results show that GBL was involved in the SEI formation, and that the SEI layer was built up from solvent as well as salt decomposition products [8].

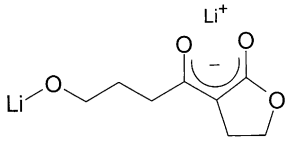

Fig. 4. Cyclic γ-alkoxy-β-keto ester Li salt, a reductive GBL decomposition product [28–32].

Combining our DEMS observations with the results just cited, we conclude that in mixed EC/GBL solutions the SEI layer is mainly built up from GBL decomposition products. Since far less EC is decomposed in the presence of GBL, the ethylene gas evolution attending EC decomposition (Eqs. (1) and (2)) is considerably diminished.

4. Conclusions

DEMS experiments performed with thick porous graphite electrodes for lithium-ion batteries have revealed protracted ethylene and hydrogen gas evolution due to decomposition of the carbonate electrolyte and to SEI formation extending beyond the first charge/discharge cycle. Because of an incomplete coulombic conversion, a high irreversible capacity, diffusion kinetics impeded by the thickness of the electrodes, and ohmic resistance in the DEMS cell, SEI formation on these thick electrodes (∼75–100 μm) was not yet *complete* after the first charge/discharge cycle. γ-Butyrolactone as a co-solvent in an EC/DMC electrolyte strongly suppressed the ethylene gas evolution associated with the formation of an SEI layer on the graphite. Here, the SEI layer was mainly built up from the decomposition products of GBL rather than from those of EC, even though the EC fraction in the electrolyte was constant at 50 wt.%.

Our experiments also demonstrated that DEMS is a powerful tool for investigating the electrochemical decomposition of electrolytes on graphite electrodes for lithium-ion batteries.

Acknowledgements

The authors thank Dr. R. Imhof (PSI, now at Renata AG), Dr. F. Joho, Dr. O. Haas and Mr. D. Goers for fruitful discussions. Ms. A.L. Corrion is acknowledged for performing part of the measurements. We also thank Dr. M.E. Spahr from TIMCAL Group, Bodio, Switzerland, for donating graphite samples and providing their characteristics and W.L. Gore & Associates GmbH, Putzbrunn, Germany, for donating the Gore-Tex membranes.

References

[1] E. Peled, in: J.-P. Gabano (Ed.), Lithium Batteries, Academic Press, London, 1983, p. 43.
[2] Y. Ein-Eli, Electrochem. Solid State Lett. 2 (1999) 212.
[3] R. Imhof, P. Novák, in: C.F. Holmes, A.R. Landgrebe (Eds.), Proceedings of the Symposium on Batteries for Portable Applications and Electric Vehicles, Vols. 97–18, The Electrochemical Society Proceedings, Pennington, NJ, 1997, p. 313.
[4] R. Imhof, P. Novák, J. Electrochem. Soc. 145 (1998) 1081.
[5] G. Eggert, J. Heitbaum, Electrochim. Acta 31 (1986) 1443.
[6] P. Novák, J.-C. Panitz, F. Joho, M. Lanz, R. Imhof, M. Coluccia, J. Power Sources 90 (2000) 52.
[7] P. Novák, F. Joho, M. Lanz, B. Rykart, J.-C. Panitz, D. Alliata, R. Kötz, O. Haas, J. Power Sources 97–98 (2001) 174–180.
[8] D. Goers, P. Novák, manuscript in preparation.
[9] M.E. Spahr, H. Wilhelm, F. Joho, P. Novák, ITE Lett. Batteries, New Technol. Med., in press.
[10] B.A. Johnson, R.E. White, J. Power Sources 70 (1998) 48.
[11] O. Haas, E. Deiss, P. Novák, W. Scheifele, A. Tsukada, in: C.F. Holmes, A.R. Landgrebe (Eds.), Proceedings of the Symposium on Batteries for Portable Applications and Electric Vehicles, Vols. 97–18, The Electrochemical Society Proceedings, Pennington, NJ, 1997, p. 451.
[12] F. Joho, B. Rykart, A. Blome, P. Novák, M.E. Spahr, IMLB-10 Abstracts Book, The Electrochemical Society, 2000, Abstract No. 76.
[13] M. Winter, P. Novák, A. Monnier, J. Electrochem. Soc. 145 (1998) 428.
[14] F. Joho, B. Rykart, R. Imhof, P. Novák, M.E. Spahr, A. Monnier, J. Power Sources 81/82 (1999) 243.
[15] S. Flandrois, B. Simon, Carbon 37 (1999) 165.
[16] B. Simon, S. Flandrois, K. Guerin, A. Fevrier-Bouvier, I. Teulat, P. Biensan, J. Power Sources 81/82 (1999) 312.
[17] K. Guerin, A. Fevrier-Bouvier, S. Flandrois, M. Couzi, B. Simon, P. Biensan, J. Electrochem. Soc. 146 (1999) 3660.
[18] M. Winter, J.O. Besenhard, M.E. Spahr, P. Novák, Adv. Mater. 10 (1998) 725.
[19] R. Imhof, P. Novák, J. Electrochem. Soc. 146 (1999) 1702.
[20] F. Joho, P. Novák, unpublished results.
[21] N. Takami, M. Sekino, T. Ohsaki, M. Kanda, M. Yamamoto, IMLB-10 Abstracts Book, The Electrochemical Society, 2000, Abstract No. 328.
[22] N. Takami, M. Sekino, T. Ohsaki, M. Kanda, M. Yamamoto, J. Power Sources 97–98 (2001) 677–680.
[23] Y. Matsuda, N. Namegaya, J. Power Sources 81 (1999) 762.
[24] D.W. Kim, Y.K. Sun, J.H. Cho, S.I. Moon, Electrochem. Solid State Lett. 2 (1999) 256.
[25] M. Kono, E. Hayashi, M. Nishiura, M. Watanabe, J. Electrochem. Soc. 147 (2000) 2517.
[26] K. Edström, M. Herranen, J. Electrochem. Soc. 147 (2000) 3628.
[27] S. Koike, T. Fujieda, N. Wakabayashi, S. Higuchi, J. Power Sources 68 (1997) 480.
[28] D. Aurbach, J. Electrochem. Soc. 136 (1989) 906, 1606, 1610.
[29] D. Aurbach, O. Chusid, J. Electrochem. Soc. 140 (1993) L1.
[30] Y. Ein-Eli, B. Markovsky, D. Aurbach, Y. Carmeli, H. Yamin, S. Luski, Electrochim. Acta 39 (1994) 2559.
[31] D. Aurbach, A. Zaban, Y. Ein-Eli, I. Weissman, O. Chusid, B. Markovsky, M. Levi, E. Levi, A. Schechter, E. Granot, J. Power Sources 68 (1997) 91.
[32] D. Aurbach, B. Markovsky, I. Weissman, E. Levi, Y. Ein-Eli, Electrochim. Acta 45 (1999) 67.